Elastic properties of Ca-based metallic glasses predicted by first-principles simulations

M. Widom,[1] B. Sauerwine,[1] A. M. Cheung,[2] S. J. Poon,[3] P. Tong,[3] D. Louca,[3] and G. J. Shiflet[2]
[1]*Department of Physics, Carnegie Mellon University, Pittsburgh, Pennsylvania 15213, USA*
[2]*Department of Materials Science and Engineering, University of Virginia, Charlottesville, Virginia 22904, USA*
[3]*Department of Physics, University of Virginia, Charlottesville, Virginia 22904, USA*
(Received 10 January 2011; revised manuscript received 7 June 2011; published 15 August 2011)

First-principles simulations of Ca-based metallic glass-forming alloys yield sample amorphous structures whose structures can be compared to experiment and whose properties can be analyzed. In an effort to understand and control ductility, we investigate the elastic moduli. Calculated Poisson ratios depend strongly on alloying elements in a manner that correlates with ionicity (charge transfer). Consequently, we predict that alloying Ca with Mg and Zn should result in relatively ductile glasses compared to alloying with Ag, Cu, or Al. Experimental observations validate these predictions.

DOI: 10.1103/PhysRevB.84.054206 PACS number(s): 61.43.Dq, 62.20.de, 62.20.fk, 71.23.Cq

I. INTRODUCTION

By adjusting alloy chemistries, metallic glasses can possess a superior wear resistance, exhibit higher strengths, and a superior resistance to corrosion compared to their equivalent crystalline compositions.[1] Amorphous alloys made predominately from light metals have attracted attention because of their low density; in particular, titanium[2] and magnesium[3] alloys. While they are lighter than ferrous-based metallic glasses, even lower density glass can be achieved with the use of calcium as the main component. Glasses made predominately from calcium are of particular interest because of this metal's very low density and relatively low materials cost. Their strength to density ratios are favorable for potential applications in the transportation and aerospace industries. Ca-based alloy systems could represent another viable avenue for designing a new class of structural materials.

While Ca-based glass alloys have low densities, the drawback with these alloys has been their tendency to be quite brittle. Improving their ductility is necessary for the alloy to be usable. Some guidelines in approaching this problem come from prior work to create Mg-based metallic glasses that were ductile.[3] With that effort and work done to improve ductility in metallic Fe-based glass by accounting for the effect of Poisson's ratio[4,5] and electronic structure,[6] it can be shown from atomistic simulations that the properties of Ca-based metallic glasses as a function of alloy composition can be predicted and improved upon based on their atomic bonding characteristics. The results are directly validated by experiment.

Computer simulation of amorphous metals requires a model for interatomic interactions. Early studies invoked pairwise interactions, either of empirical forms such as Lennard-Jones[7] or first-principles-derived.[8] Attempts to explicitly incorporate many-body interaction effects have utilized tight-binding or embedded-atom-type potentials.[9,10] The ultimate level of realism, with high sensitivity to the specific chemical natures and physical properties of constituent elements, relies on full first-principles calculations based on electronic density-functional theory.[11–14] Owing to recent advances in computational algorithms and computer speed, it is now possible to simulate systems containing hundreds of atoms that are sufficiently large to capture the short- and medium-range order of metallic glass.

We employ first-principles methods to simulate the structures of binary and ternary Ca-based metallic glasses in order to predict the impact of alloying elements on elastic properties. Structural and electronic properties of some related Ca-based glasses have been previously studied by Hafner and coworkers.[15–18] Our results suggest the alloys can be relatively ductile or brittle depending primarily on the ionicity of the interspecies interactions. As a result, we predict that alloying Ca with Mg results in greater ductility, while alloying with Cu or Al leads to greater brittleness. These predictions are supported by experimental tests of several binary alloys.

II. MOLECULAR DYNAMICS SIMULATIONS

First-principles molecular dynamics simulations utilize energies and forces calculated from first principles using electronic density-functional theory. Specifically, we use the plane-wave-based program VASP[19] in conjunction with projector-augmented-wave potentials[20] to achieve an all-electron level of accuracy, and we employ the generalized-gradient approximation to the exchange-correlation potential.[21] A sample size of 200 atoms is used for all binary and ternary alloys, guaranteeing at least 12 atoms of each species. Cubic cell dimensions of order 20 Å allow realistic short- and medium-range order at ranges up to 10 Å. Owing to the large cell size, only the Γ k point is required for the calculation of atomic forces during the molecular dynamics simulation, although we go up to a $2 \times 2 \times 2$ k-point mesh for the electronic-density-of-states calculations. Similarly, 3/4-reduced Fourier-transform grids suffice for the simulation, while we go to full-density grids to study charge transfer. We take a molecular-dynamics time step of one picosecond and utilize temperature scaling to maintain constant temperature.

To obtain accurate liquid- and amorphous-state atomic ordering, it is essential to thoroughly anneal the starting configuration at elevated temperature where atomic diffusion is rapid. For each compound, we begin annealing at $T = 2000$ K, followed by gradual reduction to our liquid-state equilibration temperature over times of two picoseconds. We then anneal at our equilibration temperature for times of at least five

TABLE I. Table of simulation data. Units are K for simulation temperature T_s, Å^3 for atomic volume V_a, GPa for bulk (K) and shear (G) moduli, states/eV/atom for density of states ρ, fractions of e for charge Q_{Ca}, and eV for COHP. Uncertainties are less than one in final digit except for shear modulus where they are listed explicitly.

Compound	T_s	V_a	K	G	ν	ρ (E_{F})	Q_{Ca}	COHP	$\Sigma_{\mathrm{Ca}X}$
Ca_3Al	973	35.1	22.7	9.5(6)	0.32	0.90	0.102	0.88	0.82
Ca_3Cu	1273	33.7	22.1	9.3(6)	0.32	0.89	0.080	0.57	0.84
Ca_3Ag	743	34.4	22.4	8.2(5)	0.34	0.88	0.071	0.68	0.85
Ca_3Zn	667	34.5	21.5	6.3(2)	0.37	1.03	0.065	0.54	0.87
Ca_3Mg	718	38.0	19.7	5.7(7)	0.37	1.07	0.054	0.56	0.92
$Ca_{12}Al_3Li$	973	35.9	20.8	7.9(8)	0.33	0.96	0.099		
$Ca_{12}Mg_3Al$	800	37.4	20.2	6.0(2)	0.37	1.03	0.066		
$Ca_{12}Mg_3La$	1000	38.9	19.5	5.6(8)	0.37	1.19	0.062		
$Ca_{12}Mg_3Zn$	1000	37.2	19.9	5.4(4)	0.38	1.07	0.057		

picoseconds. Our equilibration temperatures (see Table I) were taken approximately 200 degrees above the known or estimated liquidus temperatures for each compound. From the long equilibration runs, we selected five or more independent configurations and quenched these to create our amorphous structures. Our quench consists of a molecular dynamics simulation at temperatures dropping from the equilibration temperature down to 300 K at the rate of 1 K/fs, followed by conjugate-gradient relaxation of atomic coordinates and cell parameters, stopping when average forces fall below 10^{-2} eV/Å. The final atomic volumes are listed in Table I.

Given an amorphous structure, we wish to compute its elastic moduli. We do this by dilating and shearing the cell via the distortion matrix:

$$\begin{pmatrix} 1+\delta_V/3 & \delta_{xy}/2 & \delta_{zx}/2 \\ \delta_{xy}/2 & 1+\delta_V/3 & \delta_{yz}/2 \\ \delta_{zx}/2 & \delta_{yz}/2 & 1+\delta_V/3 \end{pmatrix}. \qquad (1)$$

We then re-relax the atomic coordinates subject to constant cell volume and shape (constant lattice vectors **a**, **b**, and **c**). We fit the energy to cubic functions of volume and shear strain and obtain the moduli from the second derivatives of the fitting functions evaluated at their minima. Specifically, we obtain bulk modulus from $K = (1/V)\partial^2 E/\partial\delta_V^2$ and the shear modulus of type $\alpha \neq \beta$ (i.e., *simple* shear) from $G_{\alpha\beta} = (1/V)\partial^2 E/\partial\delta_{\alpha\beta}^2$. Data for one representative Ca_3Mg sample are plotted in Fig. 1. Finally, we average K and G over all amorphous structures of a given composition, and average over shear types in the case of G. In general, the calculated bulk moduli of different samples are consistent to within 1% while the shear moduli differ by up to 20% among shear types and between different samples. This sample-to-sample variation and anisotropy is presumably a finite-size effect due to our 200-atom samples. Numerical values of calculated moduli, including standard deviations of shear moduli, are listed in Table I.

Additional studies can be performed with these quenched amorphous structures. We calculate their partial pair correlation functions, their electronic densities of states, and their charge densities. Charge transfer Q_{Ca} is defined as the difference between noninteracting atomic charges and fully interacting self-consistent charges, integrated over spheres of radius 2 Å surrounding each Ca atom. The electronic densities of states can be projected onto spheres surrounding each atom to obtain local and orbital-resolved densities of states. Again each of these quantities is averaged over the different amorphous structures of a given composition. The crystal orbital Hamilton population (COHP) evaluates matrix elements of the total energy between pairs of atomic orbitals on neighboring atoms.[6,22,23] COHP calculations for Ca-X bonds are carried out for crystal structures of the given or similar composition. Charge transfer measures ionicity while COHP measures the covalency of interatomic bonding. Ionicity and covalency are extreme limits of the general notion of polar bonding.

Figure 2 illustrates partial pair correlation functions for three of the binary Ca-X compounds simulated. These correlation functions have been obtained for systems at $T = 300$ K and at atomic volumes 3% greater than the quenched volumes. Notice that the Ca-Ca correlations are quite similar between the two compounds while the mixed Ca-X and X-X correlations differ significantly. In particular, the locations of the X-X peaks in $g(r)$ shift from 2.5 (X = Cu) to 2.8 (X = Al) to 3.2 Å(X = Mg) reflecting the relative sizes of the three elements. Additionally, the heights of the Ca-X peaks are greater for X = Cu and Al than for X = Mg, reflecting an

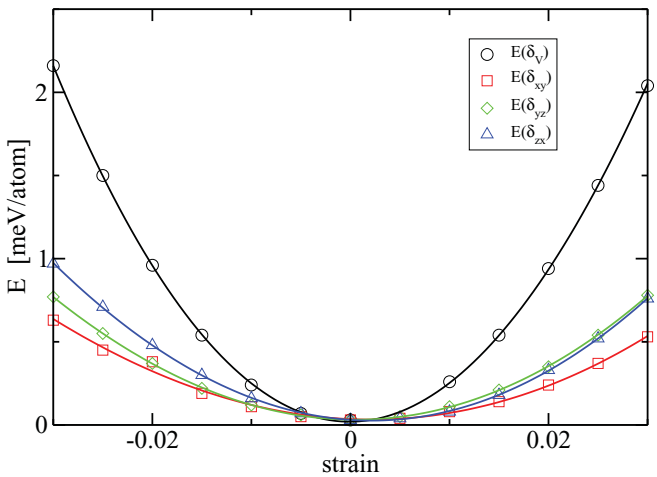

FIG. 1. (Color online) Energy vs. strain for one representative quenched amorphous sample of Ca_3Mg. Plotting symbols are calculated data points and the curves are fits to cubic polynomials.

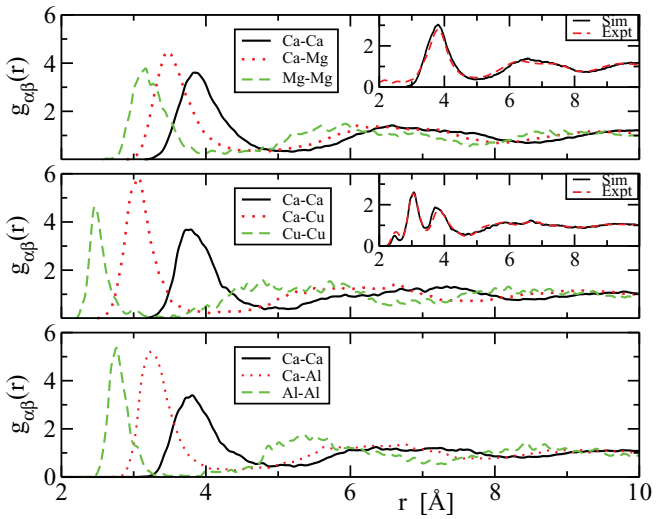

FIG. 2. (Color online) Partial pair correlation functions of Ca_3Mg (top), Ca_3Cu (middle), and Ca_3Al (bottom) glasses at $T = 300$ K. Insets compare experimental RDF with x-ray weighted sum of simulated partials.

apparently greater Ca-X binding strength of Cu and Al relative to Mg.

To explore local geometry beyond the limitations of pair correlations, we calculated Voronoi statistics for the solute atoms (minority species). Voronoi polyhedra are classified by codes (n_3,n_4,n_5, . . .) indicating the numbers of triangular, square, pentagonal, and higher faces. Code (0,3,6) indicates trigonal prisms while (0,5,4) are distorted trigonal prisms.[24] These polyhedra account for 39%, 31%, and 17% of environments, respectively, of Cu, Zn, and Ag solute atoms. In the case of Ca_3Al, 25% of Al atoms belong to Voronoi types (0,4,6) and (0,2,8), both of which occur in $Al_{14}Ca_{13}$(*mC54*). Ca_3Mg displays no particular pattern, however, the most prevalent polyhedron, with a frequency of 8%, is a distorted icosahedron (0,2,8,2). Polyhedron types are more closely governed by solute size than other bonding characteristics.

III. EXPERIMENTS

The compositions of Ca-based metallic glasses that were suggested by simulations included a ternary alloy $Ca_{12}Mg_3Al$ and several binary alloys with composition near Ca_3-X, with X being Al, Ag, Cu, Mg, or Zn. These elements positive effects on Ca-based glass formation[25] are the reason they are selected as solute additions. Alloy ingots were prepared by either alloying Ca with the other metallic elements using arc melting, induction melting, or a combination of both, in an argon atmosphere. Induction alloying was performed in a boron nitride coated graphite crucible. Ribbons of maximum thickness of 40 μm were produced by the melt-spinning method.

X-ray diffraction data were collected at the Advanced Photon Source of the Argonne National Laboratory at the 11-ID B beam line using a wavelength of 0.2127 Å. The data were collected for half an hour per sample at room temperature. The samples were sealed in quartz tubes under Ar atmosphere. They were subsequently analyzed using the pair-density-function (PDF) technique. The x-ray structure function $S(Q)$ was determined using the PDFgetX2.[26] The PDF $g/(r)$ is a real-space representation of the atomic correlations obtained through a Fourier transformation of the $S(Q)$. The highest Q_{max} employed in the analysis was 20 Å^{-1}.

Simulated x-ray PDFs were defined as

$$\mathrm{PDF}(r) = \frac{1}{\bar{Z}^2} \sum_{\alpha\beta} x_\alpha x_\beta Z_\alpha Z_\beta g_{\alpha\beta}(r) \qquad (2)$$

with the normalization factor $\bar{Z}^2 = \sum_{\alpha\beta} x_\alpha x_\beta Z_\alpha Z_\beta$ defined so that the PDF goes to 1 at large r. The excellent agreement of our simulated and experimental structures validates our simulation methods. Note that the large size difference of Cu and Ca allows us to resolve separately the three classes of near-neighbor corrrelations in the Ca-Cu binary.

The microhardness of the ribbons was determined by indenting the surface using a Vickers hardness tester with 25-gm load. The ductility of the as-spun amorphous ribbons was tested with a simple bend-and-pinch test and the trend was validated by a pull-strength test for representative alloy compositions that range from being ductile to brittle. For the pull test, a piece of ribbon was attached to the top surface of two adjoined level blocks. The blocks were then physically separated until the ribbon broke by a force normal to the adjoining surfaces. The pull test was performed to obtain a fracture surface for imaging using a JOEL 6700F scanning electron microscope (SEM).

For the pinch test, four-centimeter-long pieces of ribbon were bent until the lengthwise ends touched. Then the center of the bend of the ribbon was pinched until the inside faces of the ribbons touched. The ribbons were then held at the ends, unfolded, and pulled taunt. If the ribbons were to break during bending or during the pinch, then it was classified as "very brittle." If it broke during unfolding, it was classified as "brittle." If it could be fully unfolded and then broke when pulled taunt, it was labeled "marginal." If it survived being pulled taunt, it was classified as "ductile." The ductility rating evaluations and the density data are listed in Table II. The ductility ratings for the various compositions compare well with the theoretically predicted behavior.

The ductility of the ribbons was evaluated further by examining the plastic flow patterns on the fractured surfaces. SEM images of three pull-tested compositions selected for their different ductile classifications according to the bend-and-pinch tests were obtained. The images of the ribbon

TABLE II. Summary of ductility rating from pinch test of ribbons, calculated mass density (ρ), estimated values of σ_y from Vickers hardness test ($\sigma_y \sim 0.3$ H_v), and measured average vein spacing r_p from images of PPZs.

Composition	ρ (g/cm^3)	σ_y (MPa)	r_p (μm)	Ductility rating
Ca_3Al	1.68	433	0.2	Very Brittle
Ca_3Cu	2.17	⋯	⋯	Very Brittle
Ca_3Ag	2.60	⋯	⋯	Brittle
$Ca_{72}Zn_{28}$	2.23	⋯	⋯	Ductile
$Ca_{72}Mg_{28}$	1.58	293	1.6	Ductile
$Ca_{12}Mg_3Al$	1.60	405	0.8	Marginal

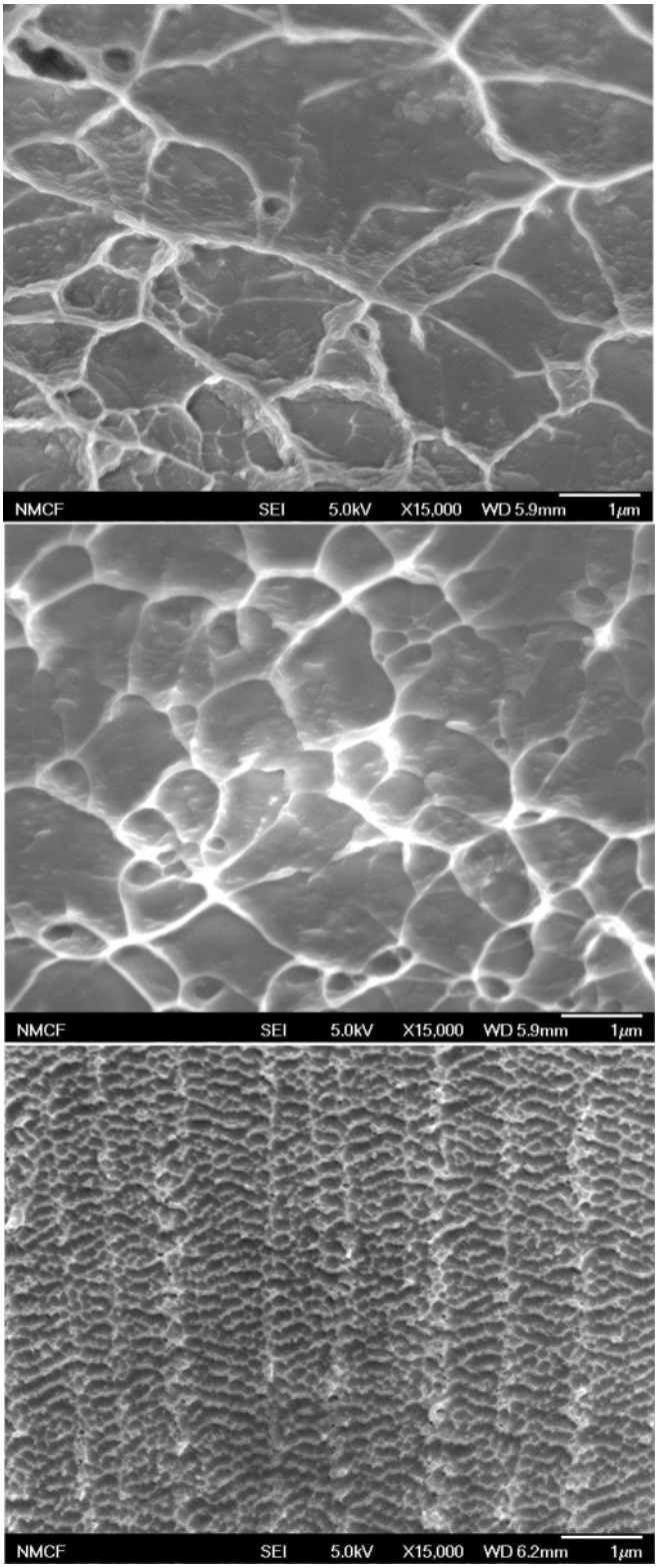

FIG. 3. SEM images of fracture surfaces. (a) $Ca_{72}Mg_{28}$, (b) $Ca_{12}Mg_3Al$, and (c) Ca_3Al.

fracture areas shown in Fig. 3 reveal the characteristic vein features of locally viscous flow and also show cell-shaped plastic processing zones (PPZ). The average size (r_p) of the PPZ has been used to characterize ductile behavior.[27] The ductility decreases as the r_p of the PPZ decreases. The r_p of each alloy viewed, listed in Table II, give indications about each alloys brittle or ductile nature.[28] The brittle ribbon $Ca_{75}Al_{25}$ had the smallest r_p while $Ca_{72}Mg_{28}$, the most ductile pull-tested ribbon, had the largest r_p, being an order of magnitude larger than the former. From SEM images of PPZ of Fe-based glass,[29,30] compared with the Ca-based glass images, similar average size r_p and structure of PPZ exists for $Ca_{72}Mg_{28}$ as well as the ductile ferrous glass. Comparable trends of size and structure can be seen when comparing the ductile Fe-based glass with ductile Ca-based glass and the brittle Fe-based glass with brittle Ca-based glass.

In addition to the PPZ structure, yield strength (σ_y) was determined for the three Ca-based alloys that were pull-tested. Strength σ_y was estimated as approximately a third of the measured hardness and values are summarized in Table II. The Ca-based σ_y values are comparable with the fracture-strength values of Mg-based amorphous alloys.[3] Although on the weaker end of fracture-strength values for metallic glasses, these Ca-based glasses have densities less than or similar to elemental Mg and fracture strengths in the same range as commercial Mg alloys (200–400 MPa).[31]

IV. DISCUSSION

Note that shear moduli vary by almost a factor of two across our compositions. Meanwhile, the bulk modulus varies by only 10%. Consequently, there is a significant variation in Poisson ratio $\nu = (3K - 2G)/(6K + 2G)$, which is believed to influence solid plasticity as suggested by Pugh.[32,33] The shear modulus also enters directly into the Rice-Thomson parameter for ductile-versus-brittle behavior.[34] The highest shear modulus and lowest Poisson ratio occur for Ca_3Al and Ca_3Cu. Indeed, these samples were reported experimentally to be the most brittle. The lowest shear modulus and highest Poisson ratio occurred for Ca_3Mg, which was also reported experimentally as the most ductile. An alternate ductility criterion based on positivity of the Cauchy pressure $P = C_{12} - C_{44}$ has been proposed for cubic structures[35,36] and translates into $P = K - 5G/3$ for isotropic materials in which $C_{12} = K = 2G/3$. Again, high bulk modulus and low shear modulus favor ductility.

We believe that the Poisson ratio is governed primarily by the degree of ionic bonding in the material. In Fig. 4, we plot calculated Poisson ratio versus calculated mean ionic charge on the Ca atoms in units of the magnitude of electron charge e. The more positive the value of Q_{Ca} the more the Ca atoms charges have been transferred to other elements in the alloy. The magnitude of charge transfer generally follows the expectations based on Pauling's electronegativity. The binary alloys have been color coded according to their reported plasticity, ranging from most ductile (red) to most brittle (blue). Notice that Zn exhibits modest Q_{Ca} and high ductility. Despite its location to the right of Cu on the periodic table, far from Mg and Ca, Zn has two outer-shell s electrons, similar to Mg and Ca, owing to its completely filled d band.

Further support for the assessment of relative binding strength comes from plots of compound enthalpies of formation (see Fig. 5). These are obtained by fully relaxing known crystal structures in each alloy family and plotting as a function of composition.[24] Stable crystal structures lie on the convex

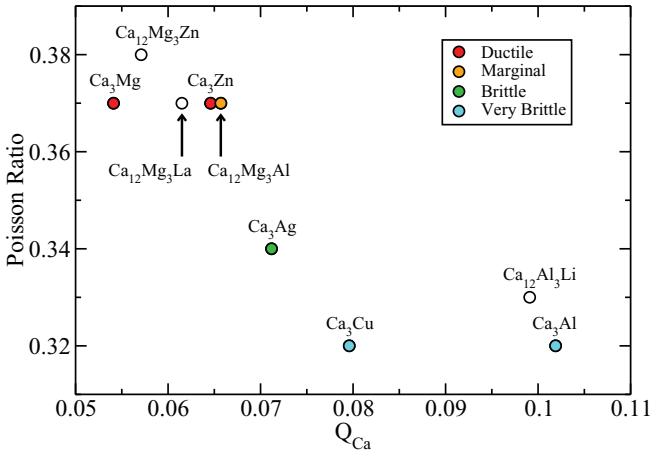

FIG. 4. (Color online) Calculated Poisson ratios (ν) as a function of charge transfer from Ca (Q_{Ca}). Experimentally tested compounds are color coded according to most ductile (red) through least ductile (blue).

hull of the plot and are indicated with heavy circles. High-temperature phases are indicated with light circles. Simulated amorphous enthalpies, indicated with diamond shapes, lie above the convex hulls, as expected, since they are metastable states. Evidently, formation enthalpies, which are indicative of interatomic bonding strength, are substantially stronger in Ca-Al and Ca-Cu than in Ca-Mg.

Additional information in Table I includes the electronic density of states at the Fermi energy $\rho(E_F)$. A high density of states is characteristic of metallic binding and a low density of states typical of covalent or ionic binding. Previously,[6,23] we have correlated the density-of-states with ductility in Fe-based metallic glasses. The trend applies here also, with the more ductile binaries having higher densities of states than the more brittle ones. The total and local densities of states for Ca_3Mg are plotted in Fig. 6, relative to the Fermi energy placed at $E = 0$. The densities of states are quite

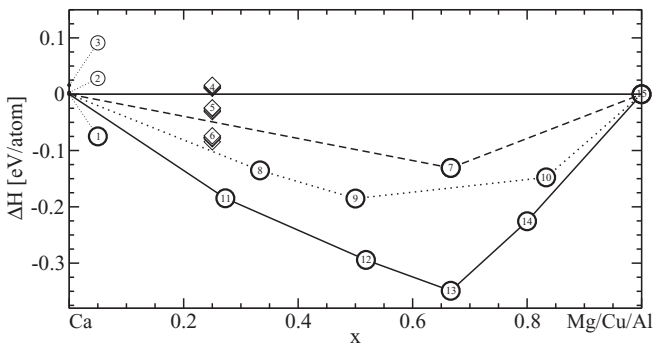

FIG. 5. Formation enthalpies of Ca-Al (solid lines), Ca-Cu (dotted lines), and Ca-Mg (dashed lines) relative to tie-line joining pure elements. Structures labeled 1–3 are elemental Ca (Pearson structure types *cF4*, *hP2*, and *cI2*, respectively); 4–6 are amorphous structures (Ca_3Mg, Ca_3Cu, and Ca_3Al, respectively); 7 is $CaMg_2$ (Pearson type *hP12*); 8 is Ca_2Cu (*oP12*); 9 is CaCu (*mP20/oP40*); 10 is $CaCu_5$ (*hP6*); 11 is Ca_8Al_3 (*aP22*); 12 is $Ca_{13}Al_{14}$ (*mC54*); 13 is $CaAl_2$ (*cF24*); 14 is $CaAl_4$ (*tI10*); 15 represents elemental Mg (*hP2*), Cu (*cF4*), and Al (*cF4*).

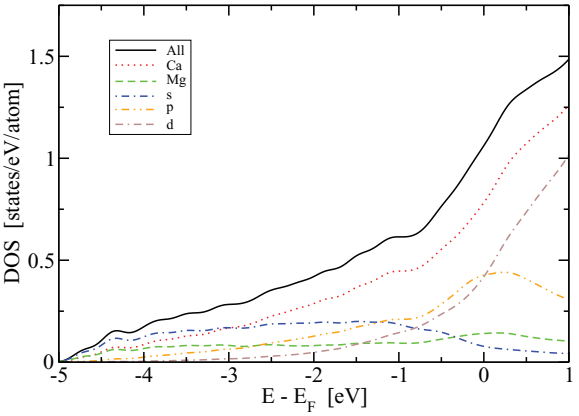

FIG. 6. (Color online) Electronic density of states of Ca_3Mg averaged over five independent samples.

free-electron-like at low energy but display an increasing d-band character in the vicinity of the Fermi energy, raising the density of states above the free-electron value as previously reported by Jaswal and Hafner.[16] Densities of states for other compounds generally resemble this plot,[17,37] except for the slight variation of the Fermi-level density of states $\rho(E_F)$ just discussed, and, of course, the presence of a localized filled d band below E_F in some cases. In no case do we observe a significant pseudogap at the Fermi level associated with a Nagel-Tauc-type stabilization.[38]

Finally, we investigate the atomic-level displacements under strain. Our deformations remain within the elastic limit, and all atomic positions return to within 0.02 Åof their initial relaxed positions upon relaxation of imposed strains. Larger deformations are required to observe irreversible displacements associated with plastic deformation. The response of individual interatomic bonds to applied strain varies in an irregular fashion among bonds. However, a trend emerges when considering the averages of near-neighbor interatomic bond lengths. Let R be the length of a bond between two atoms. Upon dilation by δ_V, the bond will stretch, and $(3/R)(\partial R/\partial \delta_V)$ measures the degree of stretching relative to an affine deformation. Hence, we define a stretching parameter

$$\Sigma_{\alpha\beta} = \left\langle \frac{3}{R}\frac{\partial R}{\partial \delta_V} \right\rangle, \tag{3}$$

where the average is taken over all bonds between atoms of type α and β within a cut-off distance defined by the first minimum of the pair correlation function $g_{\alpha\beta}(r)$. For all our binary Ca-X alloys, we find $\Sigma_{XX} < \Sigma_{\mathrm{Ca}X} < 1 < \Sigma_{\mathrm{CaCa}}$. As shown in Table I, the mixed species $\Sigma_{\mathrm{Ca}X}$ correlates strongly with charge transfer Q_{Ca}. Σ_{XX} possesses a similar correlation, though X-X bonds are few in number while Σ_{CaCa} is relatively insensitive to the alloying constituent X.

ACKNOWLEDGMENTS

This research is supported by the DARPA Structural Amorphous Metals Program under ONR Grant No. N00014-06-1-0492.

[1]M. F. Ashby and A. L. Greer, Scr. Mater. **54**, 321 (2006).
[2]F. Guo, H. Wang, S. J. Poon, and G. J. Shiflet, Appl. Phys. Lett. **86**, 091907 (2005).
[3]F. Guo, S. J. Poon, X. Gu, and G. J. Shiflet, Scr. Mater. **56**, 689 (2007).
[4]X. J. Gu, A. G. McDermott, S. J. Poon, and G. J. Shiflet, Appl. Phys. Lett. **88**, 211905 (2006).
[5]S. J. Poon, A. Zhu, and G. J. Shiflet, Appl. Phys. Lett. **92**, 261902 (2008).
[6]X. J. Gu, S. J. Poon, G. J. Shiflet, and M. Widom, Appl. Phys. Lett. **92**, 161910 (2008).
[7]P. J. Steinhardt, D. R. Nelson, and M. Ronchetti, Phys. Rev. B **28**, 784 (1983).
[8]J. Hafner, Phys. Rev. B **21**, 406 (1980).
[9]Q. K. Li and M. Li, Appl. Phys. Lett. **88**, 241903 (2006).
[10]M. I. Mendelev, D. K. Rehbein, R. T. Ott, M. J. Kramer, and D. J. Sordelet, J. Appl. Phys. **102**, 093518 (2007).
[11]H. W. Sheng, W. K. Luo, F. M. Alamgir, J. M. Bai, and E. Ma, Nature (London) **439**, 419 (2006).
[12]P. Ganesh and M. Widom, Phys. Rev. B **77**, 014205 (2008).
[13]S. Y. Wang, M. J. Kramer, M. Xu, S. Wu, S. G. Hao, D. J. Sordelet, K. M. Ho, and C. Z. Wang, Phys. Rev. B **79**, 144205 (2009).
[14]P. Ganesh and M. Widom, Phys. Rev. Lett. **102**, 075701 (2009).
[15]J. Hafner, T. Egami, S. Aur, and B. C. Giessen, J. Phys. F **17**, 1807 (1987).
[16]S. S. Jaswal and J. Hafner, Phys. Rev. B **38**, 7311 (1988).
[17]J. Hafner and S. S. Jaswal, Phys. Rev. B **38**, 7320 (1988).
[18]J. Hafner and M. Tegze, J. Phys. Condens. Matter **44**, 8277 (1989).
[19]G. Kresse and J. Furthmuller, Phys. Rev. B **54**, 11169 (1996).
[20]G. Kresse and D. Joubert, Phys. Rev. B **59**, 1758 (1999).
[21]J. P. Perdew, J. A. Chevary, S. H. Vosko, K. A. Jackson, M. R. Pederson, D. J. Singh, and C. Fiolhais, Phys. Rev. B **46**, 6671 (1992).
[22]R. Dronskowski and P. E. Blochl, J. Phys. Chem. **97**, 8617 (1993).
[23]X. J. Gu, S. J. Poon, G. J. Shiflet, and M. Widom, Acta Mater. **56**, 88 (2008).
[24]M. Mihalkovič and M. Widom, Phys. Rev. B **70**, 144107 (2004).
[25]O. N. Senkov and D. Miracle, Mater. Trans. A **39**, 1888 (2008).
[26]X. Qiu, J. W. Thompson, and S. J. L. Billinge, J. Appl. Crystallogr. **37**, 678 (2004).
[27]A. S. Argon and M. Salama, Mater. Sci. Eng. A**39**, 1888 (1976).
[28]X. K. Xi, D. Q. Zhao, M. X. Pan, W. H. Wang, Y. Wu, and J. J. Lewandowski, Phys. Rev. Lett. **94**, 125510 (2005).
[29]J. J. Lewandowski, X. J. Gu, A. S. Nouri, S. J. Poon, and G. J. Shiflet, Appl. Phys. Lett. **92**, 091918 (2008).
[30]A. S. Nouri, X. Gu, S. Poon, G. Shiflet, and J. Lewandowski, Philos. Mag. Lett. **88**, 853 (2008).
[31]G. Neite, K. Kubota, K. Higashi, and F. Hehmann, in *Structure and Properties of Nonferrous Alloys*, edited by K. H. Matucha (Wiley, New York, 1996), p. 152.
[32]S. F. Pugh, Philos. Mag. **45**, 823 (1954).
[33]J. J. Lewandowski, W. H. Wang, and A. L. Greer, Philos. Mag. Lett. **85**, 77 (2005).
[34]J. R. Rice and R. Thomson, Philos. Mag. **29**, 73 (1974).
[35]R. A. Johnson, Phys. Rev. B **37**, 3924 (1988).
[36]D. G. Pettifor, Mater. Sci. Technol. **8**, 345 (1992).
[37]M. Tegze and J. Hafner, J. Phys. Condens. Matter **44**, 8293 (1989).
[38]S. R. Nagel and J. Tauc, Phys. Rev. Lett. **35**, 380 (1975).